
This manuscript is a preprint and priory submitted for publication in GEOLOGY. Please note that subsequent versions of this manuscript may have different content. If accepted, the final version of this manuscript will be available via the 'Peer-reviewed Publication DOI' link on the right-hand side of this webpage.

Please feel free to contact any of the authors, we welcome feedback!

1 Diagenetic priming of submarine landslides in ooze-rich substrates

2 Nan Wu^{1*}, Christopher A-L. Jackson², Michael A. Clare³, David M. Hodgson⁴, Harya D. Nugraha⁵,

3 Michael J. Steventon⁶, Guangfa Zhong¹

4 ¹State Key Laboratory of Marine Geology, Tongji University, 1239 Siping Road, Shanghai, 200092,
5 China

6 ²Department of Earth and Environmental Sciences, University of Manchester, Oxford Road,
7 Manchester, M13 9PL, UK

8 ³National Oceanography Centre, Southampton SO14 3ZH, UK

9 ⁴School of Earth and Environment, University of Leeds, Leeds, LS2 9JT, UK

10 ⁵Center for Sustainable Geoscience, Universitas Pertamina, Jakarta, 12220, Indonesia

11 ⁶Shell Research, Shell Centre, London, SE1 7NA, UK

12 Email: nanwu@tongji.edu.cn

13 **Abstract**

14 Oozes are the most widespread deep-sea sediment in the global ocean, but very little is
15 known about how changes in their physical properties impact slope stability and related
16 geohazards. Characterisation of the conditions that prime ooze rich slides has been
17 hindered, as physical properties of sediments are modified by the effects of mass wasting.
18 We here use 3D seismic reflection, geochemical, and petrophysical data acquired both
19 within and adjacent to 13 large (up to c. 6330 km² in area) submarine slides on the Exmouth
20 Plateau, NW Shelf, Australia, to investigate how the pre-slide physical properties of oozes
21 control slope failure and slide emplacement. Our integrated dataset allows us to detect
22 potential slide surfaces within ooze successions; a crucial advance for improved submarine
23 geohazard assessment. Moreover, we demonstrate that the interplay of tectonics, ocean
24 current activity, and silica diagenesis can prime multiple slides on very low gradient slopes in
25 tropical, oceanic basins. We argue that the diagenesis of silica-rich sediments must be
26 accounted for in future submarine slope stability assessments.

27 Keywords: Submarine landslides; Geohazard; Diagenesis; Oozes

28 **Introduction**

29 Submarine landslides (slides) can trigger tsunami and threaten coastal communities, and
30 damage economically critically seabed infrastructure (e.g., Carter et al., 2012; Clare et al.,
31 2014; Talling et al., 2014). It is now recognized that priming substrates to fail by post-
32 depositional processes is a crucial control on their development and evolution, and that

33 instantaneous triggers, such as earthquakes, are not prerequisites for slide initiation
34 (Masson et al., 2010; Talling et al., 2014; Urlaub et al., 2018). Such preconditioning appears
35 to be particularly significant for calcareous oozes, with the biogenic constituents dominating
36 such oozes having distinct geotechnical properties and failure behaviour, being highly
37 compressible, water-rich, and prone to brittle inter-particle cementation. This potentially
38 explains why large slides occur on unusually low-angle slopes ($<2^\circ$) in areas of low sediment
39 accumulation (<0.15 m/kyr) (e.g. Gatter et al., 2021; Urlaub et al., 2018). Despite their
40 apparent significance, the pre-failure physical properties of ooze-rich slopes that ultimately
41 fail remain poorly constrained (Urlaub et al., 2018), given: (i) difficulties in directly sampling
42 and geophysically imaging the base of thick (100s m) slides; and (ii) slope failure modifies
43 the slope's pre-failure physical properties.

44 Identifying potential failure or shear surfaces within sedimentary sequences is crucial for
45 forecasting future events and modelling landslide motion (Locat et al., 2014). Previous
46 studies have mostly focused on individual slides, specifically diatomaceous, rather than
47 calcareous-ooze. Typically sampling has been from landslide debris; hence, any
48 geotechnically-weak layers are unlikely to be preserved (Gatter et al., 2021; Locat et al.,
49 2014; Urlaub et al., 2018). Therefore, the pre-emplacement physical properties of sediments
50 at basal shear surfaces remain poorly understood, given they are likely strongly modified as
51 the slide evolves (Masson et al., 2010). An understanding of the processes and timescales
52 for priming calcareous ooze-rich slides is crucial to improve geohazard assessments,
53 particularly given calcareous oozes are the most widespread deep-sea lithology ($>50\%$; see
54 Dutkiewicz et al., 2020).

55 We here integrate six time-migrated 3D seismic reflection datasets (16,189 km²; see
56 Appendix S1 for details), a regional network of 2D seismic reflection profiles, and lithological,
57 petrophysical, and geochemical data from Ocean Drilling Program (ODP) site 762 on the
58 Exmouth Plateau, NW Shelf, Australia (Figure 1A) to answer the following questions: i) what
59 are the physical properties of calcareous ooze, and can they explain the stratigraphic
60 occurrence of the basal shear surfaces of large slides? ii) to what extent does silica
61 diagenesis modify subsurface physical properties, and prime substrate for sliding?, and iii)
62 how important are regional tectonic and oceanographic controls in the preconditioning of
63 calcareous-ooze slides?

64 **Setting and Methods**

65 Seismic reflection data image 13 slides that cumulatively cover c. 6330 km² within the Upper
66 Miocene and Recent interval of the Exmouth Plateau (Horizon H2 to the seabed; Figure 1B),
67 which is equivalent to Seismic Unit 3 of Nugraha et al. (2018). ODP 762 and industrial
68 boreholes indicate this interval comprises calcareous oozes (Nugraha et al., 2018). ODP 762
69 is unaffected by sliding, but intersects an interval stratigraphically-equivalent to that hosting
70 the slides, hence we are able to characterize the pre-failure stratigraphy (Figure 2A, 2B). We
71 mapped three, age-constrained (see below) seismic horizons that define distinct changes in
72 seismic facies and thus bound two seismic units (SU1-2): (i) H1 – intra-Upper Eocene; (ii) H2
73 – the Late Miocene Unconformity (Haq et al., 1990; Nugraha et al., 2018); and (iii) H3 – an
74 undated horizon that defines the top surface of the largest slide (Slide-1; 2,800 km²), which
75 merges with H2 near the Exmouth Plateau Arch (Figure 1C). Variance attributes (see
76 Appendix S2 for explanation) were generated to determine the extent and geometry of
77 these seismic facies and inferred depositional bodies. Seismic reflection data were tied to
78 petrophysical, lithological, and geochemical data from ODP 762, allowing us correlate seismic
79 character and sediment properties (Haq et al., 1992; Scarselli et al., 2013). Velocity data
80 from ODP 762 provide a proxy record of sediment overpressure (see method outlined by
81 Dugan and Sheahan, 2012), whereas water content is used as a proxy for the sediment
82 shear strength and compressibility (Urlaub et al., 2018).

83 **Results**

84 *Horizon H1: Opal A-CT Conversion Boundary*

85 Horizon H1 defines the base of SU1 (Figure 1C). It is offset by numerous, low-throw (<20 ms
86 TWT) polygonal faults that terminate at, or just below, H2 (Figure 1B, 2C). Well-log data
87 reveal a distinct change in petrophysical properties downwards across H1, defined by a
88 sharp increase in bulk density (from 1.80 g/cm³ to 2.17 g/cm³) and velocity (from 1.62 km/s
89 to 1.86 km/s), and a decrease in porosity (from 58.0% to 42.5%) and water content (from
90 30.0% to 20.7%) (Figure 1B). This dramatic downward change in physical properties is
91 expressed in the seismic reflection data by a discrete, c. 40 ms TWT-thick package of high-
92 amplitude reflections, broadly defined at its top by a positive polarity event (i.e., a
93 downward increase in acoustic impedance; Figure 1B, 2C). X-ray diffraction measurements

94 (XRD) from ODP 762 also show that sediments above H1 have high concentrations of opal A,
95 whereas below H1, the sediment has high concentrations of opal CT (Figure 1B). H1
96 therefore corresponds to the opal A-CT conversion boundary (Haq et al., 1990; Nähr et al.,
97 1998).

98 *SU-1 - Lower Eocene to Upper Miocene chalk affected by silica diagenesis*

99 The basal part of SU-1 is enriched in clinoptilolite (Figure 1B), one of the most common
100 authigenic silicate minerals in pelagic sediments (Nähr et al., 1998). SU1 transitions upwards
101 from competent, hard chalk (Lower Eocene-Upper Eocene) to calcareous ooze (Upper
102 Eocene-Middle Miocene) (Figure 1B), and it is deformed by the polygonal fault system
103 offsetting H1 (Figure 1B, 2C). Data from ODP 762 show that the dissolved SiO₂ content
104 increases over a 50 m-thick interval near the top of SU-1 (Figure 1B). The dominant
105 diagenetic process associated with SU-1 is therefore interpreted to be silica diagenesis, with
106 the locally abundant clinoptilolite interpreted to be caused by the conversion of opal A to CT
107 (Volpi et al., 2003).

108 *Horizon H2 – Late Miocene Unconformity and regional failure plane for slides*

109 H2 defines the base of SU2 (Figure 2C and Appendix S3 for Slides 2-13). The bases of all 13
110 slides identified in this unit are on, or only 15-30 m above, H2. Well-log data from ODP 762
111 indicate H2 corresponds to a major, biostratigraphically-defined unconformity, separating
112 Late Eocene and Late Miocene deposits (Haq et al., 1990; Nugraha et al., 2018). H2 defines a
113 sharp upward increase in terrigenous particles (e.g. quartz, feldspar, and clay), and
114 nearshore coccolithophores (e.g. *Braarudosphaera Bigelow*), the latter being extremely
115 unusual for deep-marine basinal sediments, and providing possible evidence for an abrupt
116 change in the paleo-ocean current regime associated with Australia-Eurasia collision during
117 the Late Miocene (Haq et al., 1990).

118 Well-log data from ODP 762 also reveal a distinct change in petrophysical parameters across
119 H2, with bulk density increasing downward from 1.60 g/cm³ to 1.85 g/cm³, and porosity
120 decreasing downward from 80% to 58.5% (Figure 1B). The extremely low density and
121 velocity response below H2 indicates that abnormally high overpressure may have been
122 trapped below this horizon (Figure 1B; Dugan and Sheahan, 2012; Tingay et al., 2009).
123 Conversely, the locally low porosity response at the same level may indicate H2 is over-

124 compacted, with an extremely low permeability compared to the underlying sediment
125 (Figure 1B). It is these sharp changes in petrophysical properties that result in H2 being
126 expressed by a high-amplitude, negative polarity seismic reflection (Figure 1B). Another
127 petrophysically-distinct layer, Hs (c.10 m thick), immediately above H2 (Figure 1B), is
128 characterized by an upward decrease in Vp from 1.7 km/s and 1.52 km/s, and an increase in
129 water content from 30% to 48.5% (Figure 1B). The extremely low velocity response at the
130 level of Hs indicates possible underpressure at this horizon, whereas the high-water content
131 response indicates Hs has higher compressibility and lower shear strength.

132 *Seismic Unit 2: Slide-prone calcareous ooze interval affected by polygonal faulting and*
133 *dewatering*

134 SU2 contains pure calcareous ooze (Late Miocene-present) (Figure 1B) and is dominated by
135 chaotic seismic facies of highly variable amplitude. The exception to this being near ODP 762,
136 where continuous, low-amplitude reflections occur (Figure 1C). We interpret that the
137 chaotic and continuous seismic facies represent slide (e.g., Bull et al., 2009) and background
138 slope deposits, respectively. We now focus on Slide-1, the largest and best-imaged slide, to
139 investigate the role of substrate preconditioning and triggering of the slides on the Exmouth
140 Plateau (Figure 2A, 2B).

141 Below Slide-1, H1 is crosscut by numerous polygonal faults that tip-out upward at or near its
142 basal shear surface (i.e., H2; Figure 3A, 3B). H3 defines the top of Slide-1 and is a high-
143 amplitude, negative polarity reflection (Figure 3A). Directly beneath H2 are numerous high-
144 amplitude, wavy reflections that are developed close to the upper termination of the faults
145 (Figure 3A). In planform, these reflections define sub-circular (<100 m in diameter) to
146 elliptical (100-500 m long-axis length) depressions (Figure 3C), interpreted as sediment
147 accumulation (e.g. Paganoni et al., 2019). The high-amplitude wavy reflections resemble
148 zones of sediment accumulation due to fluid expulsion or gas migration as observed
149 elsewhere on the Exmouth Plateau (Foschi and Cartwright, 2020; Paganoni et al., 2019). The
150 spatial relationships between the sediment accumulation and the upper tips of polygonal
151 faults suggest the fluids driving the formation of the former migrated along the latter.

152 **Discussion and Conclusion**

153 *Controls on the formation of a regional failure surface and slide emplacement*

154 Compared with H2, the c. 10 m-thick Hs is characterized by relatively high-water content
155 (and hence low shear strength and high compressibility) and a low acoustic velocity, both
156 indicative of overpressure (Figure 4B). The geotechnical contrast between impermeable
157 strata underlying the regional H2 unconformity and the overlying water-saturated, over-
158 pressured ooze of SU2, created a weak layer, providing ideal conditions for slope failure,
159 even on very low angle slopes. We propose this explains why all thirteen slides share a
160 stratigraphically-equivalent failure surface, with Hs ultimately being locally entrained by the
161 slides.

162 A similar diagnosis was made in the shallower water Finneidfjord, Norway where multiple,
163 asynchronous fjord-flank slides share a regional failure plane, above which a low density,
164 over-pressured layer was deposited (L'Heureux et al., 2012). While the source of the weak
165 layer was terrestrially-derived mud and not deep water calcareous ooze, the similarity of a
166 highly compressible fluid-charged mud overlying an impermeable basal layer is striking.
167 Overpressure in Finneidfjord is related to the infiltration of meteoric groundwater. However,
168 such terrestrially-linked charging is not possible in the deep water setting of the Exmouth
169 Plateau, thus we discuss alternative mechanisms for overpressure development and
170 subsequent slope failure.

171 *Silica diagenesis as a primer for slope instability and failure, and slide emplacement*

172 We suggest that the most likely source for overpressure relates to the generation and
173 release of fluids during silica diagenesis, which is a well-known dehydration reaction (e.g.,
174 Davies et al., 2009; Volpi et al., 2003). The pronounced downward decrease in porosity and
175 water content below H1 suggests a large amount of fluid was expelled from the opal A-CT
176 conversion zone (Figure 4a, 4c; Davies and Clark, 2006). This fluid migrated upward, likely
177 along polygonal faults (e.g. Davies et al., 2009; Gay et al., 2006; Lüdmann et al., 2022) and
178 became trapped beneath the lower permeability Horizon H2, creating stratigraphically-
179 controlled overpressure and lowering the sediment shear strength (Figure 4B, C, D).
180 Whether such fluid migration is steady and continuous, or intermittent, perhaps triggered
181 by transient periods of seismicity, remains unclear (e.g. Embriaco et al., 2014). It is plausible
182 that enhanced seismicity, as a result of the Australian and Eurasian plates colliding during
183 the Early Miocene, could triggered fluid flow and maybe even slope failure (Nugraha et al.,
184 2018). Regardless, our findings support previous proposals of silica diagenesis priming

185 relatively local submarine slope instability and the emplacement of small, single slide (c. 110
186 km² in area; Davies and Clark, 2006; Volpi et al., 2003). Our study is the first to identify this
187 control in a tropical setting, and to show it can create a regional failure plane for multiple,
188 large volume submarine landslides.

189 *Role of tectonics and paleo-oceanography in priming and dictating the location of slope*
190 *failure*

191 During the Late Miocene, a global sea-level fall and the collision of the Australia and Eurasia
192 Plates caused the Indonesian ocean gateway to narrow offshore north Australia (Nugraha et
193 al., 2018). This caused an increase in the inflow of warm south Pacific waters, thus
194 increasing the strength of the southward flowing Leeuwin Current and suppressing the deep
195 northward-flowing Western Australia Current (Rai and Singh, 2001). These tectonically-
196 driven variations in ocean circulation fundamentally controlled the benthic and planktonic
197 foraminiferal assemblages (Srinivasan, 1985), and hence the abrupt contrast in lithology and
198 physical properties at H2 that subsequently primed submarine landslide failure depth and
199 location. The interplay of multiple physical processes on slide preconditioning can thus be
200 felt thousands, or even millions, of years after their activity has ceased (Gatter et al., 2020),
201 thus cautioning against the simplistic linkage of sliding to an external trigger. We suggest
202 that such a temporally-buffered connection likely exists for many other settings, where
203 diverse tectonic, sedimentological and/or oceanographic process interactions create
204 stratigraphically-constrained fluid sources, pathways, and permeability barriers (Gatter et al.,
205 2021; Gatter et al., 2020; L'Heureux et al., 2012).

206 **Figure Caption**

207 Figure 1. (A) Location of the study area. The red polygons and grey lines represent the 3D
208 and 2D seismic reflection data, respectively. Ocean current pathways are modified by
209 Nugraha et al. (2018). (B) Log-seismic integration at ODP 762. The lithology and age
210 correlation is interpreted from the ODP 762 scientific report (Haq et al., 1990). Direct
211 seismic to well ties between Bonaventure 3D and ODP 762 has been undertaken by Scarselli
212 et al. (2013). (C) Regional composite seismic section across the study area showing the main
213 tectonic elements and seismic units.

214 Figure 2. (A) The seabed time structure map shows the location of the thirteen slides that
215 have shaped the seabed of the study area. (B) Sketch of Figure 2A. (C) Seismic section across
216 Slide-1 shows the key seismic horizons and seismic units.

217 Figure 3. (A) Zoomed-in seismic section of Slide-1. (B) Variance time slice calculated c. 130 ms
218 below Slide-1, revealing polygonal fault systems. (C) Variance time slice calculated c. 40 ms
219 below Slide-1, showing pipe-like and crater-like structures. See the time slice location in
220 Figure 3A. See the location of Figure 3 in Figure 2B.

221 Figure 4. Schematic diagram showing the development of the slides. (A) Deposition of the
222 siliceous chalk stage. (B) Vp and water content curves at the ODP 762 reveal the potential
223 sliding surface (Hs). (C) Deposition of the calcareous oozes and opal A-CT (H1) conversion
224 stage. (D) Deposition of the regionally distributed slides stage.

225 **ACKNOWLEDGEMENTS**

226 We thank Geoscience Australia for providing the seismic data. The first author thanks the
227 Shanghai Sailing Program (Grant No. 22YF1450100) and the Fundamental Research Funds
228 for the Central Universities for their financial support.

229 **Reference**

- 230 Bull, S., Cartwright, J., and Huuse, M., 2009, A review of kinematic indicators from mass-transport
231 complexes using 3D seismic data: *Marine and Petroleum Geology*, v. 26, no. 7, p. 1132-1151.
- 232 Carter, L., Milliman, J., Talling, P., Gavey, R., and Wynn, R., 2012, Near - synchronous and delayed
233 initiation of long run - out submarine sediment flows from a record - breaking river flood,
234 offshore Taiwan: *Geophysical Research Letters*, v. 39, no. 12, p. 1-5.
- 235 Clare, M. A., Talling, P. J., Challenor, P., Malgesini, G., and Hunt, J., 2014, Distal turbidites reveal a
236 common distribution for large (> 0.1 km³) submarine landslide recurrence: *Geology*, v. 42,
237 no. 3, p. 263-266.
- 238 Davies, R., Ireland, M., and Cartwright, J., 2009, Differential compaction due to the irregular topology
239 of a diagenetic reaction boundary: a new mechanism for the formation of polygonal faults:
240 *Basin Research*, v. 21, no. 3, p. 354-359.
- 241 Davies, R. J., and Clark, I. R., 2006, Submarine slope failure primed and triggered by silica and its
242 diagenesis: *Basin Research*, v. 18, no. 3, p. 339-350.
- 243 Dugan, B., and Sheahan, T., 2012, Offshore sediment overpressures of passive margins: Mechanisms,
244 measurement, and models: *Reviews of Geophysics*, v. 50, no. 3, p. 1-20.
- 245 Dutkiewicz, A., Judge, A., and Müller, R. D., 2020, Environmental predictors of deep-sea polymetallic
246 nodule occurrence in the global ocean: *Geology*, v. 48, no. 3, p. 293-297.
- 247 Embriaco, D., Marinaro, G., Frugoni, F., Monna, S., Etiope, G., Gasperini, L., Polonia, A., Del Bianco, F.,
248 Çağatay, M. N., and Ulgen, U. B., 2014, Monitoring of gas and seismic energy release by
249 multiparametric benthic observatory along the North Anatolian Fault in the Sea of Marmara
250 (NW Turkey): *Geophysical Journal International*, v. 196, no. 2, p. 850-866.
- 251 Foschi, M., and Cartwright, J., 2020, Seal failure assessment of a major gas field via integration of
252 seal properties and leakage phenomena: *AAPG Bulletin*, v. 104, no. 8, p. 1627-1648.

253 Gatter, R., Clare, M., Kuhlmann, J., and Huhn, K., 2021, Characterisation of weak layers, physical
254 controls on their global distribution and their role in submarine landslide formation: *Earth-*
255 *Science Reviews*, v. 223, p. 103845.

256 Gatter, R., Clare, M. A., Hunt, J. E., Watts, M., Madhusudhan, B., Talling, P. J., and Huhn, K., 2020, A
257 multi-disciplinary investigation of the AFEN Slide: the relationship between contourites and
258 submarine landslides: Geological Society, London, Special Publications, v. 500, no. 1, p. 173-
259 193.

260 Gay, A., Lopez, M., Cochonat, P., Séranne, M., Levaché, D., and Sermondadaz, G., 2006, Isolated
261 seafloor pockmarks linked to BSRs, fluid chimneys, polygonal faults and stacked Oligocene–
262 Miocene turbiditic palaeochannels in the Lower Congo Basin: *Marine Geology*, v. 226, no. 1-
263 2, p. 25-40.

264 Haq, B., Boyd, R., Exon, N., and Von Rad, U., Evolution of the central Exmouth Plateau: a post-drilling
265 perspective, *in* Proceedings Proceedings of the Ocean Drilling Program, Scientific
266 Results1992, Volume 122, ODP Ocean Drilling Program, p. 801-816.

267 Haq, B., von Rad, U., and Leg, O., 1990, 122 Shipboard Scientific Party, 1990: Proc. ODP, Ink. Repts, v.
268 122, p. 9-15.

269 L'Heureux, J.-S., Longva, O., Steiner, A., Hansen, L., Vardy, M. E., Vanneste, M., Haflidason, H.,
270 Brendryen, J., Kvalstad, T. J., and Forsberg, C. F., 2012, Identification of weak layers and their
271 role for the stability of slopes at Finneidfjord, northern Norway, *Submarine mass*
272 *movements and their consequences*, Springer, p. 321-330.

273 Locat, J., Leroueil, S., Locat, A., and Lee, H., 2014, Weak layers: their definition and classification
274 from a geotechnical perspective, *Submarine mass movements and their consequences*,
275 Springer, p. 3-12.

276 Lüdmann, T., Betzler, C., Lindhorst, S., Lahajnar, N., and Hübscher, C., 2022, Submarine landsliding in
277 carbonate ooze along low-angle slopes (Inner Sea, Maldives): *Marine and Petroleum*
278 *Geology*, v. 136, p. 105403.

279 Masson, D., Wynn, R., and Talling, P., 2010, Large landslides on passive continental margins:
280 processes, hypotheses and outstanding questions, *Submarine mass movements and their*
281 *consequences*, Springer, p. 153-165.

282 Nähr, T., Botz, R., Bohrmann, G., and Schmidt, M., 1998, Oxygen isotopic composition of low-
283 temperature authigenic clinoptilolite: *Earth and Planetary Science Letters*, v. 160, no. 3-4, p.
284 369-381.

285 Nugraha, H. D., Jackson, C. A. L., Johnson, H. D., Hodgson, D. M., and Reeve, M. T., 2018, Tectonic
286 and oceanographic process interactions archived in Late Cretaceous to Present deep -
287 marine stratigraphy on the Exmouth Plateau, offshore NW Australia: *Basin Research*, v. 31,
288 no. 3, p. 405-430.

289 Paganoni, M., King, J. J., Foschi, M., Mellor-Jones, K., and Cartwright, J. A., 2019, A natural gas
290 hydrate system on the Exmouth Plateau (NW shelf of Australia) sourced by thermogenic
291 hydrocarbon leakage: *Marine and Petroleum Geology*, v. 99, p. 370-392.

292 Rai, A., and Singh, V., 2001, Late Neogene deep-sea benthic foraminifera at ODP Site 762B, eastern
293 Indian Ocean: diversity trends and palaeoceanography: *Palaeogeography, Palaeoclimatology,*
294 *Palaeoecology*, v. 173, no. 1-2, p. 1-8.

295 Scarselli, N., McClay, K., and Elders, C., 2013, Submarine slide and slump complexes, Exmouth
296 Plateau, NW Shelf of Australia, *in* Proceedings The Sedimentary Basins of Western Australia
297 IV: Proceedings of the Petroleum Exploration Society of Australia Symposium, Perth,
298 WA2013, Volume 18.

299 Srinivasan, K. J. K. G., 1985, Miocene planktonic foraminiferal biogeography and pale-oceanographic
300 development of the Indo-Pacific region: *The Miocene Ocean: Paleoceanography and*
301 *biogeography: Boulder, Colorado Geologic Society of America Memoir*, p. 197-236.

302 Talling, P. J., CLARE, M. L., Urlaub, M., Pope, E., Hunt, J. E., and Watt, S. F., 2014, Large submarine
303 landslides on continental slopes: geohazards, methane release, and climate change:
304 Oceanography, v. 27, no. 2, p. 32-45.

305 Tingay, M. R., Hillis, R. R., Swarbrick, R. E., Morley, C. K., and Damit, A. R., 2009, Origin of
306 overpressure and pore-pressure prediction in the Baram province, Brunei: Aapg Bulletin, v.
307 93, no. 1, p. 51-74.

308 Urlaub, M., Geersen, J., Krastel, S., and Schwenk, T., 2018, Diatom ooze: Crucial for the generation of
309 submarine mega-slides?: Geology, v. 46, no. 4, p. 331-334.

310 Volpi, V., Camerlenghi, A., Hillenbrand, C. D., Rebesco, M., and Ivaldi, R., 2003, Effects of biogenic
311 silica on sediment compaction and slope stability on the Pacific margin of the Antarctic
312 Peninsula: Basin Research, v. 15, no. 3, p. 339-363.

Figure 1

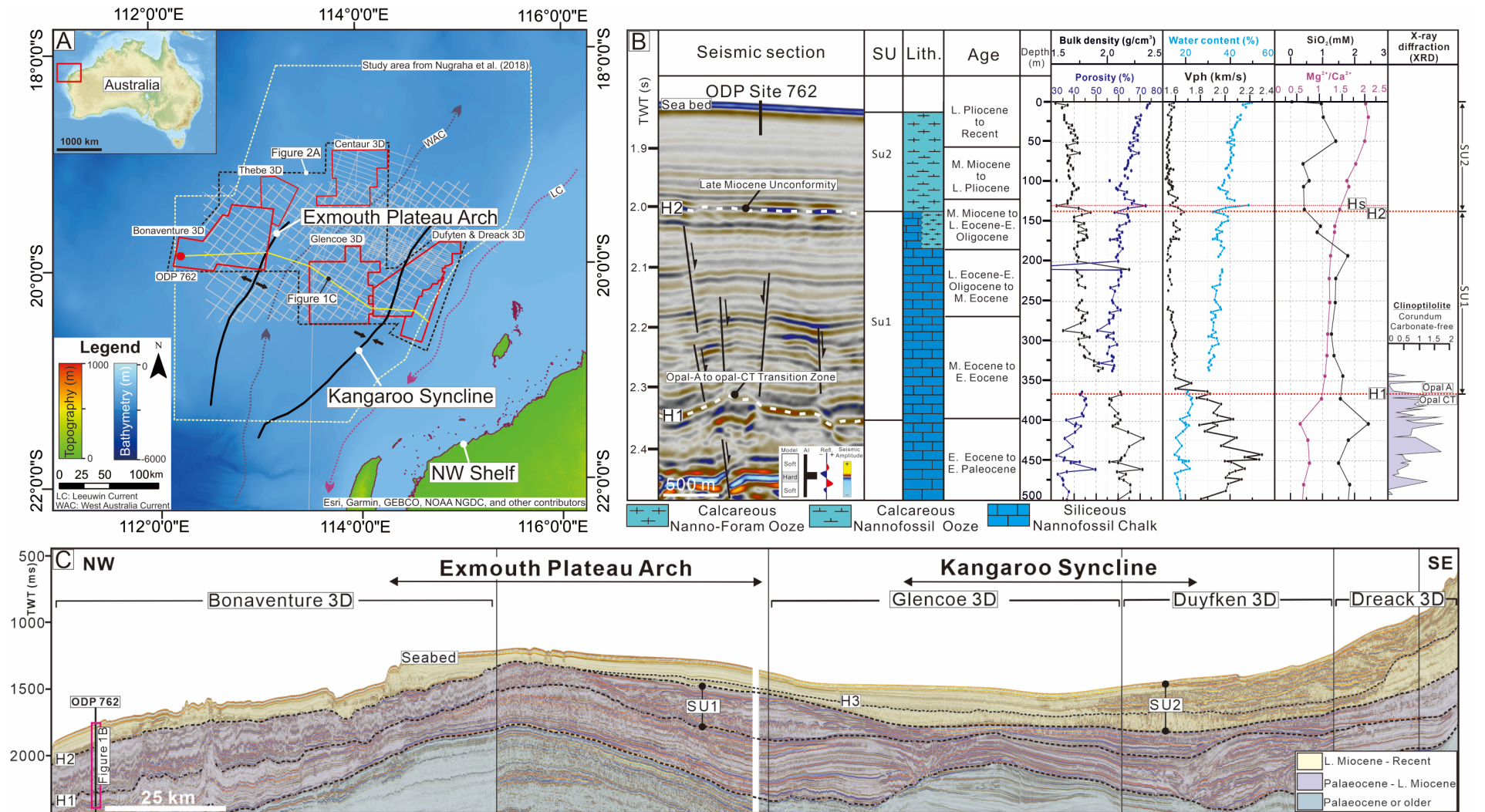


Figure 2

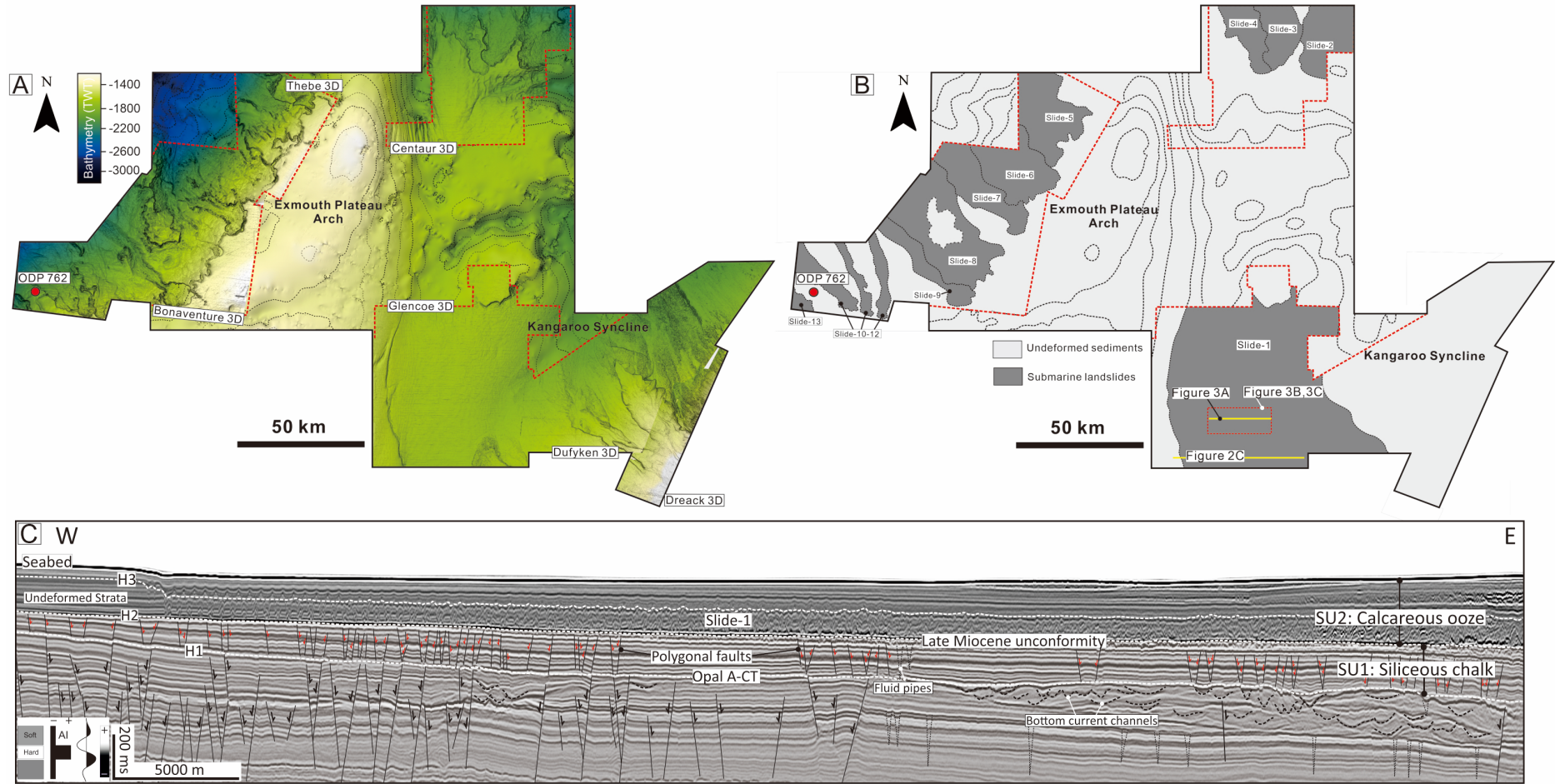


Figure 3

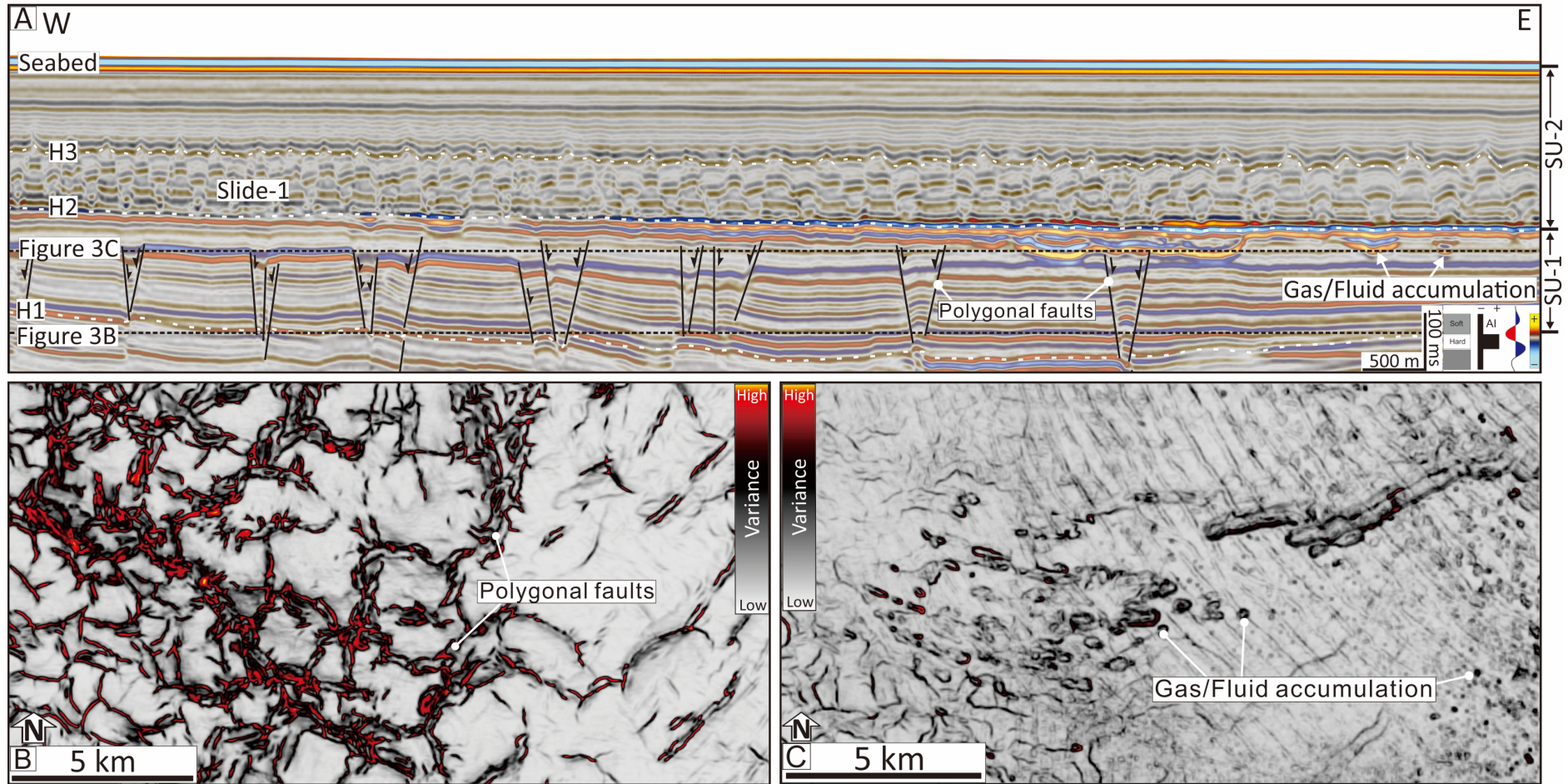


Figure 4

